Commun. Comput. Phys.
doi: 10.4208/cicp.091012.120813a

Vol. **15**, No. 3, pp. 569-595
March 2014

Numerical Validation for High Order Hyperbolic Moment System of Wigner Equation

Ruo Li[1,2,4], Tiao Lu[1,2,4,*], Yanli Wang[1,3,4] and Wenqi Yao[1]

[1] *School of Mathematical Sciences, Peking University, Beijing 100871, P.R. China.*
[2] *HEDPS and LMAM, Peking University, Beijing 100871, P.R. China.*
[3] *BICMR, Peking University, Beijing 100871, P.R. China.*
[4] *CAPT, Peking University, Beijing 100871, P.R. China.*

Received 9 October 2012; Accepted (in revised version) 12 August 2013

Available online 18 October 2013

Abstract. A globally hyperbolic moment system upto arbitrary order for the Wigner equation was derived in [6]. For numerically solving the high order hyperbolic moment system therein, we in this paper develop a preliminary numerical method for this system following the NRxx method recently proposed in [8], to validate the moment system of the Wigner equation. The method developed can keep both mass and momentum conserved, and the variation of the total energy under control though it is not strictly conservative. We systematically study the numerical convergence of the solution to the moment system both in the size of spatial mesh and in the order of the moment expansion, and the convergence of the numerical solution of the moment system to the numerical solution of the Wigner equation using the discrete velocity method. The numerical results indicate that the high order moment system in [6] is a valid model for the Wigner equation, and the proposed numerical method for the moment system is quite promising to carry out the simulation of the Wigner equation.

AMS subject classifications: 82C10, 81-08, 47A57

Key words: Wigner equation, NRxx method, moment method.

1 Introduction

The Wigner equation was proposed by Wigner in 1932 to study the quantum corrections of the quantum statistical mechanics [41]. For its strong similarity with the classical counterpart of the Boltzmann equation, the Wigner equation has advantages in simulating the

*Corresponding author. *Email addresses:* rli@math.pku.edu.cn (R. Li), tlu@math.pku.edu.cn (T. Lu), wangyanliwyl@gmail.com (Y. Wang), albee0926@sina.com (W. Yao)

carrier transport in semiconductor devices [14]. Its applications are also found in quantum chemistry and quantum optics. So there has been an increasing interest in the Wigner equation.

The numerical methods for the Wigner equation have attracted many researchers from different fields. In [15], Frensley applied the upwind finite difference method to the Wigner equation, and successfully showed the negative differential resistance of the resonant tunneling diodes (RTD). Further, the finite difference methods for the Wigner equation have been used to investigate the Wigner-Poisson equations [23, 42]. Readers may refer [24, 28] for the comparison study of different finite difference methods for the Wigner equation. Besides the popular finite difference methods for the Wigner equation, many other numerical methods have been proposed. For example, [35] has given a new adaptive cell average spectral element method for the time-dependent Wigner equation. An operator splitting [1], a Fourier spectral method [34], and a Monte Carlo method [32] have also been put forward. Analysis and numerical solution for the discrete version of the transient Wigner equation have been given in [17, 18].

Though the Wigner functions have been successfully used in simulating one-dimensional devices, but are not expected to be directly used for the multi-dimensional devices simulation using deterministic numerical methods due to its formidable expense in memory storage and computation time. One practical approach to investigate higher dimensional devices where the quantum effects are relevant is to use the quantum hydrodynamics models which are moment systems derived from the Wigner equation. Because the close connection between the Wigner equation and the Boltzmann equation, many moment methods devised for the Boltzmann equation have been extended to the Wigner equation [13, 16]. The equations derived from the Wigner equation are called quantum drift-diffusion equations, quantum Euler equations and quantum hydrodynamics equations. Moreover, the numerical simulations based on such moment equations are extensively studied [12, 22, 26, 27, 43].

The moment method of the Boltzmann equation can be dated back to Grad [19] in 1940s. However, this 13-moment model proposed therein was soon found to be problematic [20]. Its major deficiencies include the appearance of subshocks in the structure of a strong shock wave and the loss of global hyperbolicity. A number of regularizations were raised to solve or alleviate these problems [25, 29, 37–39]. However, due to the complexity of the explicit expressions, systems with large number of moments are not investigated until recently (see, for examples, [2, 40]). In [4, 5], a new regularized model with global hyperbolicity is proposed by the correction of the characteristic speed and numerical methods solving large moment systems were proposed in [7, 8, 10].

Recently, we have extended the method of the hyperbolic regularization in [4, 5] to the Wigner equation, and obtained a new set of generalized quantum hydrodynamic models [6]. In this paper, we are aiming at developing an effective numerical solver for the quantum hydrodynamic models deduced therein. Since the quantum hydrodynamic model is a moment expansion, which may be truncated up to any order, our method can numerically solve it in a unified way which is actually able to be regarded as a kind

of spectral method by expanding the Wigner function into the Hermite functions in the microscopic velocity space. The method is basically following the techniques in [8]. The appealing properties, including the numerical conservation of the total mass and the total momentum, are proved in our numerical method, while the variation of the total energy is under perfectly control. The numerical convergence in the number of moments indicates that the moment system is a valid model for the Wigner equation. The numerical efficiency is significantly improved compared to solving the Wigner equation using the discrete velocity method since we can use only tens of moments to achieve enough numerical accuracy. However, we have assumed that the potential is smooth enough.

The rest of this paper is arranged as follows: in Section 2 we introduce the moment system derived in [6]. The numerical discretization scheme is proposed in Section 3 as well as the proof of the conservative properties. Section 4 provides several numerical results to show the numerical convergence. Concluding remarks are in the last section.

2 Hyperbolic moment system of the Wigner equation

Let $f(t,x,p)$ denote the quasi-probability density function in the phase space (x,p). We can write the Wigner equation in the 1D spatial space and 1D microscopic velocity space (which will be called 1D-1D Wigner equation for short hereafter) with the scattering term as follows

$$\frac{\partial f}{\partial t}+\frac{p}{m}\frac{\partial f}{\partial x}+\Theta[V]f=\left.\frac{\partial f}{\partial t}\right|_{\text{Scat}},\quad x\in\mathbb{R},\quad p\in\mathbb{R}, \tag{2.1}$$

where the effective mass m is taken to be $m=1$ for convenience and the nonlocal Wigner potential term $\Theta[V]f$ is a pseudo-differential operator. It is defined by

$$(\Theta[V]f)(t,x,p)=\int_{\mathbb{R}}V_w(t,x,p')f(t,x,p-p')\,\mathrm{d}p', \tag{2.2}$$

and the Wigner potential V_w is given as

$$V_w(t,x,p)=\frac{-\mathrm{i}}{2\pi\hbar^2}\int_{\mathbb{R}}[V(t,x+\frac{y}{2})-V(t,x-\frac{y}{2})]e^{\mathrm{i}yp/\hbar}\,\mathrm{d}y, \tag{2.3}$$

where $\hbar$ is the Planck constant, i is the complex unit and $V(t,x)$ is the electric potential energy (which will be called potential for short hereafter). The pseudo-operator $\Theta[V]f$ can be written into an equivalent form

$$(\Theta[V]f)(t,x,p)=-\sum_{\lambda=1,3,5,\cdots}\frac{(\hbar/2\mathrm{i})^{\lambda-1}}{\lambda!}\frac{\partial^\lambda V}{\partial x^\lambda}\frac{\partial^\lambda f}{\partial p^\lambda}, \tag{2.4}$$

where λ is odd [6,21].

Remark 2.1. The self-consistent electrostatic potential are added to $V(x)$ in the simulation of semiconductor devices [1]. But in the current framework of this paper the acceleration

due to the potential involving its high order derivatives, it is not trivial to couple the nonlinear effect into the system yet. With a second order numerical method solving the Poisson equation numerically, only its first order derivative can still have a first order accuracy. Thus in order to focus on showing the convergence of the numerical solution to the solution of the Wigner equation as our main object in this paper, we assume that $V(x,t)$ is a given smooth function.

The time-relaxation approximation of the scattering term, which is the same as the BGK scattering term used for the collision gas [3], is applied here [15]

$$\left.\frac{\partial f}{\partial t}\right|_{\text{Scat}} = \frac{f_{\text{eq}} - f}{\tau}, \tag{2.5}$$

where τ is the relaxation time and f_{eq} is the equilibrium distribution. For example, when the density of the electrons is not extremely high, we can assume that the equilibrium distribution is a Maxwellian distribution,

$$f_{\text{eq}} = \frac{\rho(t,x)}{(2\pi k_B T(t,x))^{1/2}} \exp\left(-\frac{(p-u(t,x))^2}{2k_B T(t,x)}\right), \tag{2.6}$$

where $\rho(t,x)$ is the number density of the particles at position x, k_B is the Boltzmann constant, $T(t,x)$ is the particle temperature, and $u(t,x)$ is the average momentum of the particles. These macroscopic variables are related with the distribution function as below

$$\rho(t,x) = \int_{\mathbb{R}} f(t,x,p)\,\mathrm{d}p, \tag{2.7a}$$

$$\rho(t,x)u(t,x) = \int_{\mathbb{R}} p f(t,x,p)\,\mathrm{d}p, \tag{2.7b}$$

$$\rho(t,x)k_B T(t,x) = \int_{\mathbb{R}} (p-u)^2 f(t,x,p)\,\mathrm{d}p. \tag{2.7c}$$

The conservation of mass, momentum and total energy can be derived from the Wigner equation. Multiplying Eq. (2.1) by 1 and p respectively, then integrating with respect to x and p, we have

$$\frac{\mathrm{d}}{\mathrm{d}t}\int_{\mathbb{R}\times\mathbb{R}} f(t,x,p)\,\mathrm{d}x\mathrm{d}p = 0, \quad t\in\mathbb{R}^+, \tag{2.8a}$$

$$\frac{\mathrm{d}}{\mathrm{d}t}\int_{\mathbb{R}\times\mathbb{R}} p f(t,x,p)\,\mathrm{d}x\mathrm{d}p = -\int_{\mathbb{R}} \rho(t,x)\frac{\partial V(t,x)}{\partial x}\,\mathrm{d}x, \quad t\in\mathbb{R}^+. \tag{2.8b}$$

Multiplying Eq. (2.1) by p^2 and integrating by parts, we get the conservation of the total energy

$$\frac{\mathrm{d}}{\mathrm{d}t}\int_{\mathbb{R}\times\mathbb{R}} p^2 f(t,x,p)\,\mathrm{d}x\mathrm{d}p = -2\int_{\mathbb{R}} \rho(t,x)u(t,x)\frac{\partial V(t,x)}{\partial x}\,\mathrm{d}x, \quad t\in\mathbb{R}^+. \tag{2.9}$$

2.1 Moment expansion

Following the same method in [6,7,10], we expand the distribution function into Hermite series as

$$f(t,x,p)=\sum_{\alpha\in\mathbb{N}} f_\alpha(t,x)\mathcal{H}_{\mathcal{T},\alpha}\left(\frac{p-u(t,x)}{\sqrt{\mathcal{T}(t,x)}}\right), \tag{2.10}$$

where the basis functions $\mathcal{H}_{\mathcal{T},\alpha}$ are the Hermite functions defined by

$$\mathcal{H}_{\mathcal{T},\alpha}(\xi)=\frac{1}{\sqrt{2\pi}}\mathcal{T}^{-\frac{\alpha+1}{2}}He_\alpha(\xi)\exp\left(-\frac{\xi^2}{2}\right), \tag{2.11}$$

where $He_n(x)$ is the Hermite polynomial of order n, and the parameter $\mathcal{T}$ in the expansion is the scaled local temperature defined as

$$\mathcal{T}(t,x)=k_BT(t,x). \tag{2.12}$$

Using the orthogonality properties of the Hermite polynomials, we can obtain that $\rho(t,x)=f_0(t,x)$ from (2.7a) and (2.10). Direct calculation from (2.7b), (2.7c) and (2.10) yields $f_1=0$ and $f_2=0$. Then from (2.6), (2.5) and (2.10), the time-relaxation approximation scattering term (2.5) can be expanded into Hermite series as [6,15]

$$\left.\frac{\partial f}{\partial t}\right|_{\text{Scat}}=\frac{1}{\tau}(f_{\text{eq}}-f)=-\frac{1}{\tau}\sum_{\alpha\geqslant 3} f_\alpha\mathcal{H}_{\mathcal{T},\alpha}\left(\frac{p-u(t,x)}{\sqrt{\mathcal{T}(t,x)}}\right). \tag{2.13}$$

The heat flux q and the pressure P are defined as

$$q=\frac{1}{2}\int_{\mathbb{R}}(p-u)^3f\,\mathrm{d}p,\quad P=\int_{\mathbb{R}}(p-u)^2f\,\mathrm{d}p, \tag{2.14}$$

and replacing f with (2.10) yields

$$q=3f_3,\quad P=\rho\mathcal{T}. \tag{2.15}$$

2.2 Moment closure

In this paper, we follow the method in [5, 6] to derive the moment system. The final moment system for the 1D-1D Wigner equation is as below [6]:

$$\frac{\partial\rho}{\partial t}+u\frac{\partial\rho}{\partial x}+\rho\frac{\partial u}{\partial x}=0, \tag{2.16a}$$

$$\rho\frac{\partial u}{\partial t}+\rho u\frac{\partial u}{\partial x}+\frac{\partial P}{\partial x}=-\rho\frac{\partial V}{\partial x}, \tag{2.16b}$$

$$\frac{\partial P/2}{\partial t}+u\frac{\partial P/2}{\partial x}+\frac{3}{2}P\frac{\partial u}{\partial x}+3\frac{\partial f_3}{\partial x}=0, \tag{2.16c}$$

$$\frac{\partial f_\alpha}{\partial t}+\left(\frac{P}{\rho}\frac{\partial f_{\alpha-1}}{\partial x}+u\frac{\partial f_\alpha}{\partial x}+(\alpha+1)\frac{\partial f_{\alpha+1}}{\partial x}\right)+\frac{\partial u}{\partial x}\left(\frac{P}{\rho}f_{\alpha-2}+(\alpha+1)f_\alpha-\frac{P}{\rho}f_{\alpha-2}\right)$$
$$-\frac{f_{\alpha-1}}{\rho}\frac{\partial P}{\partial x}-\frac{1}{\rho}f_{\alpha-2}\frac{\partial q}{\partial x}+\left(-\frac{P}{2\rho^2}\frac{\partial \rho}{\partial x}+\frac{1}{2\rho}\frac{\partial P}{\partial x}\right)\left(\frac{P}{\rho}f_{\alpha-3}+(\alpha+1)f_{\alpha-1}\right)$$
$$=-\frac{1}{\tau}f_\alpha-\sum_{\lambda=1,3,\cdots}\frac{(\hbar/2\mathrm{i})^{\lambda-1}}{\lambda!}\frac{\partial^\lambda V}{\partial x^\lambda}f_{\alpha-\lambda},\quad \alpha\geqslant 3. \tag{2.16d}$$

A closure of the above infinite set of equations is given in [5,6]. Picking an integer $M\geqslant 3$, we truncate the expansion (2.10) at order M. Then disregarding the equations which contain $\partial f_\alpha/\partial t$ with $\alpha>M$, and adopting the regularization given in [5], we obtain the closed final moment system as follows

$$\frac{\partial \boldsymbol{w}}{\partial t}+\hat{\mathbf{M}}(\boldsymbol{w})\frac{\partial \boldsymbol{w}}{\partial x}=\mathbf{G}\boldsymbol{w}+\mathbf{S}\boldsymbol{w}, \tag{2.17}$$

where $\boldsymbol{w}=(\rho,u,P/2,f_3,\cdots,f_M)^T$ and $\hat{\mathbf{M}}$ is an $(M+1)\times(M+1)$ matrix given by

$$\hat{\mathbf{M}}(\boldsymbol{w})\frac{\partial \boldsymbol{w}}{\partial x}=\mathbf{M}(\boldsymbol{w})\frac{\partial \boldsymbol{w}}{\partial x}-\mathcal{R}_M I_M, \tag{2.18}$$

where $\mathbf{M}(\boldsymbol{w})$ is an $(M+1)\times(M+1)$ matrix, whose entries are given as the coefficients of the terms in (2.16a), (2.16b), (2.16c) and (2.16d) with derivatives of $\boldsymbol{w}$, and $\mathcal{R}_M I_M$ is the regularization term [6], with $I_M=(0,\cdots,0,1)^T\in\mathbb{R}^{M+1}$ and $\mathcal{R}_M$ defined as

$$\mathcal{R}_M=(M+1)\left[f_M\frac{\partial u}{\partial x}+\frac{1}{2}f_{M-1}\frac{\partial \mathcal{T}}{\partial x}\right]. \tag{2.19}$$

Moreover, the entries of $\mathbf{G}$ arise from the non-local Wigner potential term (2.4) and the explicit formula is

$$\mathbf{G}_{ij}=\begin{cases}-\frac{1}{\rho}\frac{\partial V(t,x)}{\partial x}, & \text{if } i=2,\ j=1,\\ -\frac{(\hbar/2\mathrm{i})^{i-j-1}}{(i-j)!}\frac{\partial^{i-j}V(t,x)}{\partial x^{i-j}}, & \text{if } 3\leq i\leq M+1,\ i-j \text{ is odd},\ j\neq 2,3,\\ 0, & \text{otherwise.}\end{cases} \tag{2.20}$$

The entry $\mathbf{S}_{ij}$ of $\mathbf{S}$ arises from the scattering term (2.13) and it takes the nonzero value $-\frac{1}{\tau}$ only when $i=j$ and $i\geq 4$.

We list the detailed moment system of (2.17) when $M=5$ as an example. (2.16a), (2.16b), and (2.16c) are the first three equations of this moment system, and the else three

equations are

$$\begin{aligned}
&\frac{\partial f_3}{\partial t}-\frac{P^2}{2\rho^2}\frac{\partial \rho}{\partial x}+4f_3\frac{\partial u}{\partial x}+\frac{P}{2\rho}\frac{\partial P}{\partial x}+u\frac{\partial f_3}{\partial x}+4\frac{\partial f_4}{\partial x}=-\frac{1}{\tau}f_3+\frac{\hbar^2}{24}\frac{\partial^3 V}{\partial x^3}\rho,\\
&\frac{\partial f_4}{\partial t}-\frac{5}{2}\frac{P}{\rho^2}f_3\frac{\partial \rho}{\partial x}+5f_4\frac{\partial u}{\partial x}-\frac{f_3}{\rho}\frac{\partial P}{\partial x}+\frac{P}{\rho}\frac{\partial f_3}{\partial x}+u\frac{\partial f_4}{\partial x}+5\frac{\partial f_5}{\partial x}=-\frac{f_4}{\tau},\\
&\frac{\partial f_5}{\partial t}-\frac{f_4}{\rho}\frac{\partial P}{\partial x}-\frac{3f_3}{\rho}\frac{\partial f_3}{\partial x}+\frac{P}{\rho}\frac{\partial f_4}{\partial x}+u\frac{\partial f_5}{\partial x}=-\frac{f_5}{\tau}+\frac{\hbar^4}{1920}\frac{\partial^5 V}{\partial x^5}\rho,
\end{aligned}$$

where $\frac{\hbar^2\rho}{24}\frac{\partial^3 V}{\partial x^3}$ and $\frac{\hbar^4\rho}{1920}\frac{\partial^5 V}{\partial x^5}$ are the quantum correction terms yielded by the non-local Wigner potential term (2.4) [6].

Remark 2.2. By [5], the regularized moment system (2.17) is globally hyperbolic, thus is locally well-posed for certain small initial value.

3 Numerical method

The numerical scheme for the regularized moment system (2.17) is a natural extension of the first order method in [8, 11]. In this paper, we focus on our major effort of the validation of the model, saying to study if the high order moment system will successfully provide a solution approaching the kinetic equation, we would rather adopt a reliable numerical scheme than provide a high order numerical scheme with better efficiency. We would like to give a simple comment on high-order methods here. There are actually some essential difficulties in developing a high order scheme since we have no idea at all for us to reconstruct a high order numerical approximation by the cell means. Just as in numerically solving an Euler equation, one can reconstruct derivatives in a cell using conservative variables, or using primitive variables, or some other possible approaches. For the high order moment method, the amount of choices in the approaches to reconstruct the high order approximation is even huge. This trapped us in the situation that we do not know which choice is the best since there are too many candidates. We can not provide any convincing arguments that one of these candidates is better than another yet.

By using a first order Strang-splitting method [36], we split the moment system into the following parts:

- the convection step:

$$\frac{\partial \boldsymbol{w}}{\partial t}+\hat{\mathbf{M}}(\boldsymbol{w})\frac{\partial \boldsymbol{w}}{\partial x}=0, \tag{3.1}$$

- the acceleration and scattering step:

$$\frac{\partial \boldsymbol{w}}{\partial t}=(\mathbf{G}+\mathbf{S})\boldsymbol{w}. \tag{3.2}$$

A second order time splitting algorithm can be given by considering additional steps [30].

The numerical scheme adopted in the x-direction is the standard finite volume discretization. Suppose Γ_h to be a uniform mesh in $\mathbb{R}$, and each cell is identified by an index j. For a fixed $x_0 \in \mathbb{R}$ and $\Delta x > 0$,

$$\Gamma_h = \left\{ \mathrm{T}_j = x_0 + (j\Delta x,\ (j+1)\Delta x) : j \in \mathbb{Z} \right\}. \tag{3.3}$$

The approximation of the coefficients of the Hermite expansion of the distribution function f at $t = t_n$ is denoted as

$$f_\alpha^n(x) = f_{\alpha,j}^n, \quad x \in \mathrm{T}_j, \tag{3.4}$$

where $f_{\alpha,j}^n$ is the approximation over the cell T_j at the n-th time step and then the discrete distribution function has the following Hermite expansion form

$$f_h^n(x,p) = f_j^n(p) = \sum_{|\alpha| \leqslant M} f_{\alpha,j}^n \mathcal{H}_{\mathcal{T}_j^n,\alpha}\left(\frac{p - u_j^n}{\sqrt{\mathcal{T}_j^n}} \right). \tag{3.5}$$

3.1 The convection step

Following [6], we can find that the term $\mathbf{M}(\boldsymbol{w})$ comes from the conservative part in the Grad-type moment system, while the term $\mathcal{R}_M I_M$ only revises f_M. Therefore solving (3.1) is equal to firstly solving the original form of the convection part of the Wigner equation, which reads

$$\frac{\partial f}{\partial t} + p\frac{\partial f}{\partial x} = 0, \tag{3.6}$$

and then applying the regularization in [5] on f. Here the distribution function f is approximated as (3.5), and (3.6) is discretized as

$$f_j^{n+1,*}(p) = f_j^n(p) + K_{1,j}^n(p) + K_{2,j}^n(p), \tag{3.7}$$

where $K_{1,j}^n$ is the contribution of the term $\mathbf{M}(\boldsymbol{w})$ in (2.18) and $K_{2,j}^n$ is the contribution of the term $\mathcal{R}_M I_M$ in (2.19). Here $K_{1,j}^n$ is discretized in the conservative formation as

$$K_{1,j}^n(p) = -\frac{\Delta t^n}{\Delta x}\left[F_{j+\frac{1}{2}}^n(p) - F_{j-\frac{1}{2}}^n(p) \right], \tag{3.8}$$

where $F_{j+\frac{1}{2}}^n$ is the numerical flux between cell T_j and T_{j+1} at t^n. We use the HLL scheme in our numerical experiments following [9], which reads:

$$F_{j+\frac{1}{2}}^n(p) = \begin{cases} p f_j^n(p), & 0 \leqslant \lambda_{j+\frac{1}{2}}^L, \\ \dfrac{\lambda_{j+\frac{1}{2}}^R p f_j^n(p) - \lambda_{j+\frac{1}{2}}^L p f_{j+1}^n(p) + \lambda_{j+\frac{1}{2}}^L \lambda_{j+\frac{1}{2}}^R [f_{j+1}^n(p) - f_j^n(p)]}{\lambda_{j+\frac{1}{2}}^R - \lambda_{j+\frac{1}{2}}^L}, & \lambda_{j+\frac{1}{2}}^L < 0 < \lambda_{j+\frac{1}{2}}^R, \\ p f_{j+1}^n(p), & 0 \geqslant \lambda_{j+\frac{1}{2}}^R, \end{cases} \tag{3.9}$$

where $\lambda^L_{j+\frac{1}{2}}$ and $\lambda^R_{j+\frac{1}{2}}$ are defined in (3.16).

As for the regularization part, the DLM theory [31,33] is employed to define the weak solution since it is non-conservative. The regularization term $\mathcal{R}_M I_M$ only revises the coefficient f_M, therefore, only when $\alpha = M$, we have to calculate $K^n_{2,j}$. Here we follow the method in [8]. Considering a non-conservative system as

$$\frac{\partial \boldsymbol{q}}{\partial t}+\frac{\partial \boldsymbol{F}(\boldsymbol{q})}{\partial x}+\mathbf{N}(\boldsymbol{q})\frac{\partial \boldsymbol{q}}{\partial x}=0,$$

a cluster of integral paths $\boldsymbol{\Phi}(s;\cdot,\cdot)$, where $s\in[0,1]$ is the parameter of the paths, has to be additionally given in the phase space to define the shock condition (generalized Rankine-Hugoniot condition)

$$\boldsymbol{F}(\boldsymbol{q}_L)-\boldsymbol{F}(\boldsymbol{q}_R)+\int_0^1 [v_s\mathbf{I}-\mathbf{N}(\boldsymbol{\Phi}(s;\boldsymbol{q}_L,\boldsymbol{q}_R))]\frac{\partial \boldsymbol{\Phi}}{\partial s}(s;\boldsymbol{q}_L,\boldsymbol{q}_R)\,\mathrm{d}s=0, \tag{3.10}$$

where $\boldsymbol{q}_L$ and $\boldsymbol{q}_R$ are the left and right states connected by a shock wave with shock speed v_s, and $\mathbf{I}$ is the identity matrix. About other restrictions on the paths $\boldsymbol{\Phi}(s;\cdot,\cdot)$, we refer the readers to [33] for more information.

For the particular case under our consideration here, entries of $\mathbf{N}$ are all vanished except for the last row to be

$$\left(0,(M+1)f_M,\frac{M+1}{2}f_{M-1},0,\cdots,0\right).$$

We take the integral path $\boldsymbol{\Phi}(s;\cdot,\cdot)$ in the phase space to be linear, saying

$$\boldsymbol{\Phi}(s;\boldsymbol{w}_L,\boldsymbol{w}_R)=(1-s)\boldsymbol{w}_L+s\boldsymbol{w}_R.$$

Thus $K^n_{2,j}$ is chosen as the form below following [8]

$$K^n_{2,j}=-\frac{\Delta t}{\Delta x}(\hat{W}^{n-}_{j+1/2}-\hat{W}^{n+}_{j-1/2})\mathcal{H}_{\mathcal{T}^n_j,M}\left(\frac{p-u^n_j}{\mathcal{T}^n_j}\right), \tag{3.11}$$

where $\hat{W}^{n\pm}_{j+1/2}$ is defined by

$$\hat{W}^{n-}_{j+1/2}=\begin{cases}0, & 0\leqslant\lambda^L_{j+1/2},\\ -\frac{\lambda^L_{j+1/2}}{\lambda^R_{j+1/2}-\lambda^L_{j+1/2}}g^n_{j+1/2}, & \lambda^L_{j+1/2}<0<\lambda^R_{j+1/2},\\ g^n_{j+1/2}, & 0\geqslant\lambda^R_{j+1/2},\end{cases} \tag{3.12}$$

and

$$\hat{W}^{n+}_{j+1/2}=\begin{cases}-g^n_{j+1/2}, & 0\leqslant\lambda^L_{j+1/2},\\ -\frac{\lambda^R_{j+1/2}}{\lambda^R_{j+1/2}-\lambda^L_{j+1/2}}g^n_{j+1/2}, & \lambda^L_{j+1/2}<0<\lambda^R_{j+1/2},\\ 0, & 0\geqslant\lambda^R_{j+1/2},\end{cases} \tag{3.13}$$

where

$$g^n_{j+1/2}=\int_0^1 (M+1)\begin{pmatrix} (1-s)f_{M,j}+sf_{M,j+1} \\ \frac{1-s}{2}f_{M-1,j}+\frac{s}{2}f_{M-1,j+1}\end{pmatrix}^T \begin{pmatrix} \frac{\partial[(1-s)u_j+su_{j+1}]}{\partial s} \\ \frac{\partial[(1-s)\mathcal{T}_j+s\mathcal{T}_{j+1}]}{\partial s}\end{pmatrix} \mathrm{d}s, \tag{3.14}$$

which results

$$g^n_{j+1/2}=(M+1)\left[\begin{pmatrix} f^n_{M,j}/2 \\ f^n_{M-1,j}/4\end{pmatrix}+\begin{pmatrix} f^n_{M,j+1}/2 \\ f^n_{M-1,j+1}/4\end{pmatrix}\right]^T \begin{pmatrix} u^n_{j+1}-u^n_j \\ \mathcal{T}^n_{j+1}-\mathcal{T}^n_j\end{pmatrix}. \tag{3.15}$$

The $\lambda^L_{j+\frac{1}{2}}$ and $\lambda^R_{j+\frac{1}{2}}$ above are the greatest eigenvalues of $\hat{M}$ (see [5]) as

$$\lambda^L_{j+\frac{1}{2}}=\min\{u^n_j-C_{M+1}\sqrt{\mathcal{T}^n_j},u^n_{j+1}-C_{M+1}\sqrt{\mathcal{T}^n_{j+1}}\}, \tag{3.16a}$$

$$\lambda^R_{j+\frac{1}{2}}=\max\{u^n_j+C_{M+1}\sqrt{\mathcal{T}^n_j},u^n_{j+1}+C_{M+1}\sqrt{\mathcal{T}^n_{j+1}}\}, \tag{3.16b}$$

where C_{M+1} is the greatest zero of $He_{M+1}(x)$. The formula of the signal speed is also used to determine the time step Δt^n by the CFL condition

$$\frac{\Delta t^n}{\Delta x}\max_j\{|\lambda^R_{j+1/2}|,|\lambda^L_{j+1/2}|\}<\mathrm{CFL}. \tag{3.17}$$

Remark 3.1. There are two points remaining unclear in calculation of the numerical flux (3.9), one is how to calculate $pf^n_j(p)$ and the other is how to add up two distribution functions with the expansion center $(u_1,\mathcal{T}_1)$ and $(u_2,\mathcal{T}_2)$ respectively. The techniques on these two points have been clarified in detail in [11].

3.2 The acceleration and scattering step

With the coefficients $\boldsymbol{w}^{n+1,*}_j$ of $f^{n+1,*}_{j,\alpha}$ obtained from (3.7), we then solve (3.2) with $\boldsymbol{w}^{n+1,*}_j$ as the initial value at t^n for the acceleration and scattering step. Since $\mathbf{G}+\mathbf{S}$ is a lower triangular matrix, (3.2) can be easily solved using the implicit Euler method

$$\frac{\boldsymbol{w}^{n+1}_j-\boldsymbol{w}^{n+1,*}_j}{\Delta t^n}=(\mathbf{G}+\mathbf{S})_j\boldsymbol{w}^{n+1}_j, \tag{3.18}$$

where $(\mathbf{G}+\mathbf{S})_j$ is the volume average of $(\mathbf{G}+\mathbf{S})$ in the j-th cell. In (3.18), only one point needs to be clarified. By the definition of $\mathbf{G}$ and $\mathbf{S}$ (see the context around (2.20)), it can be seen that the first three rows of $(\mathbf{G}+\mathbf{S})$ in (3.2) exactly have only one non-zero entry $G_{2,1}=-\frac{1}{\rho}\frac{\partial V}{\partial x}$. Thus u can be updated before updating the else entries of $\boldsymbol{w}^{n+1,*}$ by solving

$$\frac{\partial u}{\partial t}=-\frac{\partial V(t,x)}{\partial x}. \tag{3.19}$$

For the time step Δt^n, (3.19) is approximated as

$$u_j^{n+1} = u_j^{n+1,*} - \Delta t^n V_j', \tag{3.20}$$

where V_j' is the volume average of $\frac{\partial V(t,x)}{\partial x}$ in the j-th cell at t^n.

Remark 3.2. Eq. (3.19) shows the effect of the first order derivative of the potential $V(t,x)$ on the momentum of the particles in the classical system. It is clear that the scattering and the high-order derivatives of the potential $V(t,x)$ only change f_α with $3 \leqslant \alpha \leqslant M$, and does not change the density ρ, the momentum u and the temperature $\mathcal{T}$, which are determined by the coefficients with $\alpha \leqslant 2$.

3.3 Outline of the algorithm

Suppose the coefficient $\boldsymbol{w}_j^n$, $j = 1, \cdots, N$, of $f_{\alpha,j}^n$ has been obtained, we summarized the overall numerical scheme for one time step as follows:

1. Calculate Δt^n according to the CFL condition using (3.17);
2. Obtain $f_{\alpha,j}^{n+1,*}$ by integrating the convection term using (3.7) and thus obtain $\boldsymbol{w}_j^{n+1,*}$;
3. Obtain u_j^{n+1} by computing the classical acceleration term using (3.20);
4. Obtain $f_{\alpha,j}^{n+1}, \alpha \geq 3$ by computing the quantum acceleration and scattering term using (3.18). Since $\rho_j^{n+1} = \rho_j^{n+1,*}$ and $P_j^{n+1} = P_j^{n+1,*}$, we have obtained $\boldsymbol{w}_j^{n+1}$.

3.4 The conservative properties of the scheme

In this subsection, we will study the properties of the scheme. Let us denote the discretized mass as

$$\mathcal{D}_h(t_n) = \sum_{j=1}^{N} \Delta x \int_{p \in \mathbb{R}} f_j^n(p)\,\mathrm{d}p, \tag{3.21}$$

the discretized momentum as

$$\mathcal{M}_h(t_n) = \sum_{j=1}^{N} \Delta x \int_{p \in \mathbb{R}} p f_j^n\,\mathrm{d}p, \tag{3.22}$$

the total impulse due to the potential at the n-th time step as

$$\mathcal{F}_h(t_n) = -\sum_{j=1}^{N} \Delta x \Delta t^n V_j' \rho_j^{n+1}, \tag{3.23}$$

the discretized total energy as

$$\mathcal{E}_h(t_n)=\sum_{j=1}^{N}\Delta x\int_{p\in\mathbb{R}}p^2 f_j^n \mathrm{d}p, \tag{3.24}$$

and the total work done by the potential at the n-th time step as

$$\mathcal{W}_h(t^n)=-2\sum_{j=1}^{N}\Delta x\Delta t^n\rho_j^{n+1,*}u_j^{n+1,*}V_j'. \tag{3.25}$$

Direct calculation gives us the following conclusion.

Theorem 3.1. *The numerical solution $f_h^n(x,p)$ given by the scheme satisfies that:*

1. *Conservation of total mass: $\mathcal{D}_h(t_n)=\mathcal{D}_h(t_0)$;*
2. *Conservation of total momentum: $\mathcal{M}_h(t_n)=\mathcal{M}_h(t_0)+\sum_{k=0}^{n-1}\mathcal{F}_h(t_k)$;*
3. *Variation of total energy:*

$$\mathcal{E}_h(t^{n+1})=\mathcal{E}_h(t^n)+\mathcal{W}_h(t^n)+\mathcal{O}(\Delta t^2), \tag{3.26}$$

in the case of the periodic boundary condition.

Proof. We check these three items one by one.

1. Conservation of mass:

Noticing that the mass on each cell is not modified when we apply the regularization term and in the acceleration and scattering step, the conservation of the mass is straight forward based on results in [9].

2. Conservation of momentum:

For the momentum conservation, we need only verify

$$\mathcal{M}_h(t_{n+1})=\mathcal{M}_h(t_n)+\mathcal{F}_h(t_n). \tag{3.27}$$

In the calculation of the acceleration and scattering step, only the acceleration step (3.19) changes the momentum. So we verify below that the momentum is conserved in the acceleration step and the convection step, respectively.

(a) We first verify that the acceleration step keeps momentum to be conservative. From

(3.22) and (3.20), we have

$$\begin{aligned}\mathcal{M}_h(t_{n+1}) &= \Delta x\sum_{j=1}^{N}\rho_j^{n+1}u_j^{n+1}\\ &= \Delta x\sum_{j=1}^{N}\rho_j^{n+1}\left(u_j^{n+1,*}-V_j'\Delta t^n\right)\\ &= \Delta x\sum_{j=1}^{N}\rho_j^{n+1}u_j^{n+1,*}-\Delta x\Delta t^n\sum_{j=1}^{N}V_j'\rho_j^{n+1}\\ &= \Delta x\sum_{j=1}^{N}\rho_j^{n+1}u_j^{n+1,*}+\mathcal{F}_h(t_n).\end{aligned}\tag{3.28}$$

Since ρ_j^{n+1} is the density after the n-th convection step, $\Delta x\sum_{j=1}^{N}\rho_j^{n+1}u_j^{n+1,*}$ is the total momentum after the n-th convection step.

(b) Next we verify that the convection step does not change the total momentum. Thanks to (2.7b) and (3.7), we have

$$\begin{aligned}&\Delta x\sum_{j=1}^{N}\rho_j^{n+1}u_j^{n+1,*}=\sum_{j=1}^{N}\Delta x\int_{p\in\mathbb{R}}pf_j^{n+1,*}\mathrm{d}p\\ &=\sum_{j=1}^{N}\Delta x\int_{p\in\mathbb{R}}p[f_j^n+K_{1,j}^n+K_{2,j}^n]\mathrm{d}p\\ &=\sum_{j=1}^{N}\Delta x\int_{p\in\mathbb{R}}pf_j^n\mathrm{d}p+\sum_{j=1}^{N}\Delta x\int_{p\in\mathbb{R}}pK_{1,j}^n\mathrm{d}p+\sum_{j=1}^{N}\Delta x\int_{p\in\mathbb{R}}pK_{2,j}^n\mathrm{d}p\\ &=\sum_{j=1}^{N}\Delta x\int_{p\in\mathbb{R}}pf_j^n\mathrm{d}p-\Delta t^n\sum_{j=1}^{N}\int_{p\in\mathbb{R}}p(F_{j+1/2}^n-F_{j-1/2}^n)\mathrm{d}p+\sum_{j=1}^{N}\Delta x\int_{p\in\mathbb{R}}pK_{2,j}^n\mathrm{d}p\\ &=\mathcal{M}_h(t_n)-\Delta t^n\int_{p\in\mathbb{R}}p(F_{N+1/2}^n-F_{1/2}^n)\mathrm{d}p+\sum_{j=1}^{N}\Delta x\int_{p\in\mathbb{R}}pK_{2,j}^n\mathrm{d}p,\end{aligned}\tag{3.29}$$

which gives

$$\Delta x\sum_{j=1}^{N}\rho_j^{n+1}u_j^{n+1,*}=\mathcal{M}_h(t_n),\tag{3.30}$$

because $K_{2,j}$ defined in (3.11) are orthogonal to p, and $F_{N+1/2}^n=F_{1/2}^n$ due to the periodic boundary condition. With (3.28) and (3.30), we conclude the total momentum conservation consequently

$$\mathcal{M}_h(t_{n+1})=\mathcal{M}_h(t_n)+\mathcal{F}_h(t_n).\tag{3.31}$$

3. Variation of total energy:

For the total energy is only related to $(\rho,u,\mathcal{T})$, it is clear that the scattering term does not change the total energy, and the potential term does not change ρ and $\mathcal{T}$

$$\rho_j^{n+1,*}=\rho_j^{n+1},\quad \mathcal{T}_j^{n+1}=\mathcal{T}_j^{n+1,*}, \tag{3.32}$$

where $\rho_j^{n+1,*}$ and $\mathcal{T}_j^{n+1,*}$ is the density ρ and the local temperature $\mathcal{T}$ at the j-th cell after the n-th convection step. Similar to the proof in the momentum conservation, the variation of the total energy will be verified in the potential step and the convection step respectively.

(a) We first compute the variation of the total energy in the potential step. Thanks to (2.7c) and (3.20), we have

$$\begin{aligned}
\mathcal{E}_h(t^{n+1})&=\sum_{j=1}^{N}\Delta x\int_{p\in\mathbb{R}}p^2f_j^{n+1}\mathrm{d}p\\
&=\sum_{j=1}^{N}\Delta x\big(\rho_j^{n+1}(u_j^{n+1})^2+\rho_j^{n+1}\mathcal{T}_j^{n+1}\big)\\
&=\sum_{j=1}^{N}\Delta x\big(\rho_j^{n+1,*}(u_j^{n+1})^2+\rho_j^{n+1,*}\mathcal{T}_j^{n+1,*}\big)\\
&=\sum_{j=1}^{N}\Delta x\rho_j^{n+1,*}\left(u_j^{n+1,*}-\Delta tV_j'\right)^2+\sum_{j=1}^{N}\Delta x\rho_j^{n+1,*}\mathcal{T}_j^{n+1,*}\\
&=\sum_{j=1}^{N}\Delta x\big(\rho_j^{n+1,*}(u_j^{n+1,*})^2+\rho_j^{n+1,*}\mathcal{T}_j^{n+1,*}\big)-2\sum_{j=1}^{N}\Delta x\Delta t^n\rho_j^{n+1,*}u_j^{n+1,*}V_j'\\
&\quad+\sum_{j=1}^{N}\Delta x(\Delta t^n)^2\rho_j^{n+1,*}(V_j')^2,\\
&=\sum_{j=1}^{N}\Delta x\big(\rho_j^{n+1,*}(u_j^{n+1,*})^2+\rho_j^{n+1,*}\mathcal{T}_j^{n+1,*}\big)+\mathcal{W}_h(t^n)+\mathcal{O}(\Delta t^2).
\end{aligned}\tag{3.33}$$

Since

$$\mathcal{E}_h(t^{n+1,*})=\sum_{j=1}^{N}\Delta x\big(\rho_j^{n+1,*}(u_j^{n+1,*})^2+\rho_j^{n+1,*}\mathcal{T}_j^{n+1,*}\big)$$

is the total energy after the n-th convection step, it is deduced that

$$\mathcal{E}_h(t^{n+1})=\mathcal{E}_h(t^{n+1,*})+\mathcal{W}_h(t^n)+\mathcal{O}(\Delta t^2). \tag{3.34}$$

(b) Then we show that the convection step does not change the total energy. Precisely, we have

$$\begin{aligned}\mathcal{E}_h(t^{n+1,*}) &= \sum_{j=1}^{N}\Delta x\int_{p\in\mathbb{R}} p^2 f_j^{n+1,*}\mathrm{d}p\\ &= \sum_{j=1}^{N}\Delta x\int_{p\in\mathbb{R}} p^2 f_j^{n}\mathrm{d}p+\sum_{j=1}^{N}\Delta x\int_{p\in\mathbb{R}} p^2 K_{1,j}^{n}\mathrm{d}p+\sum_{j=1}^{N}\Delta x\int_{p\in\mathbb{R}} p^2 K_{2,j}^{n}\mathrm{d}p\\ &= \mathcal{E}_h(t_n)-\Delta t^n\sum_{j=1}^{N}\int_{p\in\mathbb{R}} p^2(F_{j+1/2}^{n}-F_{j-1/2}^{n})\mathrm{d}p+\sum_{j=1}^{N}\Delta x\int_{p\in\mathbb{R}} p^2 K_{2,j}^{n}\mathrm{d}p\\ &= \mathcal{E}_h(t_n)-\Delta t^n\int_{p\in\mathbb{R}} p(F_{N+1/2}^{n}-F_{1/2}^{n})\mathrm{d}p+\sum_{j=1}^{N}\Delta x\int_{p\in\mathbb{R}} p^2 K_{2,j}^{n}\mathrm{d}p. \qquad (3.35)\end{aligned}$$

Making use of the orthogonality of p^2 and $K_{2,j}$, we have

$$\mathcal{E}_h(t^{n+1,*}) = \mathcal{E}_h(t^n). \qquad (3.36)$$

Collecting (3.34) and (3.36), we then conclude the variation of the total energy consequently is as

$$\mathcal{E}_h(t^{n+1}) = \mathcal{E}_h(t^n)+\mathcal{W}_h(t^n)+\mathcal{O}(\Delta t^2). \qquad (3.37)$$

The proof is complete. □

Remark 3.3. When $V(t,x)$ is time-independent, i.e., $V(t,x)=V(x)$, u^{n+1} obtained by (3.20) is exact, and the work done by the potential from t^n to t^{n+1} defined in (3.25) can be revised into

$$\mathcal{W}_h(t^n) = -2\sum_{j=1}^{N}\Delta x\Delta t^n\rho_j^{n+1,*}V_j'(u_j^{n+1,*}-\Delta t^n V_j'/2).$$

The exact conservation of energy is obtained by comparison the extra term in the revised definition with the error term in (3.33), thus

$$\mathcal{E}_h(t^{n+1}) = \mathcal{E}_h(t^n)+\mathcal{W}_h(t^n).$$

4 Numerical examples

In this section, we study the numerical convergence of the scheme applied to the 1D-1D Wigner equation (2.1) with a BGK scattering term (2.5). For simplicity, we take its nondimensional form by taking the Planck constant $\hbar=1$ and the Boltzmann constant $k_B=1$. The CFL number is always set as 0.45. Here we adopt the initial data as below

$$f_0(x,p) = f_{\mathrm{eq}}(x,p) = \frac{\rho_0(x)}{\sqrt{2\pi\mathcal{T}_0(x)}}\exp\left(\frac{(p-u_0(x))^2}{2\mathcal{T}_0(x)}\right),\quad (x,p)\in(L_l,L_r)\times\mathbb{R}, \qquad (4.1)$$

where $\rho_0(x)$, $u_0(x)$, and $\mathcal{T}_0(x)$ are the initial density, momentum, and local temperature, respectively. The initial data is chosen as below

$$\rho_0(x)=\exp(-(x-25)^2)+0.1, \quad u_0(x)=10, \quad \mathcal{T}_0(x)=0.5, \tag{4.2}$$

and the potential is set to be

$$V=10\exp(-x^2/200), \quad x\in(-100,200).$$

The reference solution is provided by the discretized velocity method using $\Delta x=0.00625$ as the spatial gird size, $\Delta v=0.0125$ as the velocity grid size on the velocity interval $[-20,20]$. The numerical methods is the classical finite volume method using upwinding numerical flux. The discretized velocity computation is very time consuming while the accuracy of the solution on such a grid is comparatively reliable by our numerical resolution study.

4.1 Numerical convergence study for classical system

In this subsection, we first will apply the numerical method we proposed to the Wigner equation with only classical acceleration. That means, we first consider the Boltzmann equation, which is the classical counterpart of the Wigner equation.

Firstly, we examine the numerical convergence with different spatial grid sizes. The 1D-1D Boltzmann equation with and without the scattering term is numerically solved. We fix the number of moments to be 25 and use the spatial meshes with grid size $\Delta x=0.4$, 0.2, 0.1, 0.05 and 0.025.

In the first example, the system without the scattering term is considered. In Figs. 1 and 2, the density ρ, macroscopic momentum u, local temperature $\mathcal{T}$ and heat flux q at $t=3$ and $t=6$ are plotted. As the spatial grid size decreases, ρ, u and $\mathcal{T}$ obtained by solving the moment system with $M=25$ converge to the reference values given by the discrete velocity method. In Fig. 3, the L_1 error of ρ, u, $\mathcal{T}$ and q at $t=3$ and $t=6$ are plotted, respectively. All errors are about linearly converging to zero with the decreasing of the spatial grid size.

In the second example, we consider the system with a BGK scattering term (2.5) with $\tau=1/2$. The results of ρ, u, $\mathcal{T}$ and q obtained with different grid sizes and the result of the discrete velocity method at $t=3$ and $t=6$ are plotted in Figs. 4 and 5. Comparison of it with Figs. 1 and 2 shows that the movement the scattering slows down the movement of particles. At the same time, the results in Figs. 4 and 5 illustrate that ρ, u, $\mathcal{T}$ and q also converge to the reference values obtained with the discrete velocity method, respectively. Its L_1 errors plotted in Fig. 6 also converge about linearly to zero with the decreasing of the spatial grid size.

Secondly, let us turn to the study of the numerical convergence in terms of the number of moments. We would like to point out that a scattering term generally gives a more smooth distribution function and the numerical convergence with the increase of the

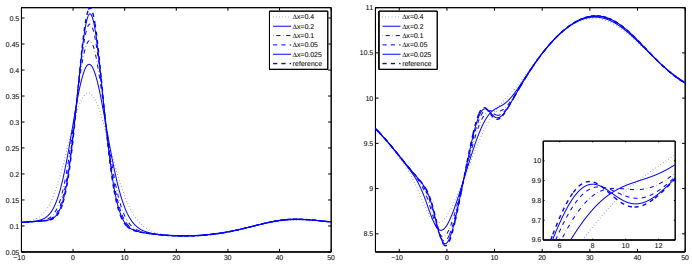

(a) ρ at $t=3$ (b) u at $t=3$

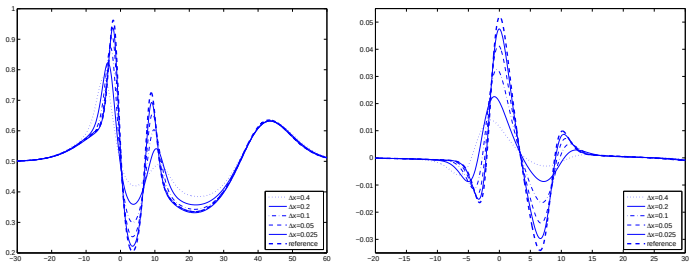

(c) $\mathcal{T}$ at $t=3$ (d) q at $t=3$

Figure 1: The density ρ and macroscopic momentum u, local temperature $\mathcal{T}$ and heat flux q of the 1D-1D Wigner equation with only the classical acceleration and without the scattering term on different spatial grids at $t=3$. The thick dashed line is the reference solution.

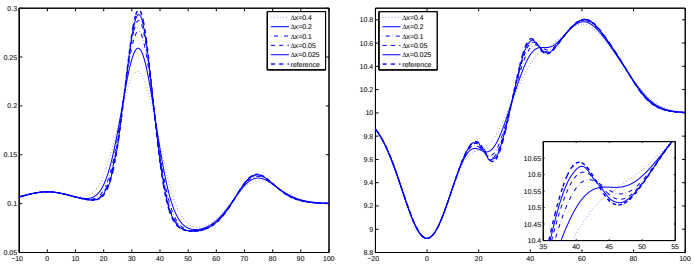

(a) ρ at $t=6$ (b) u at $t=6$

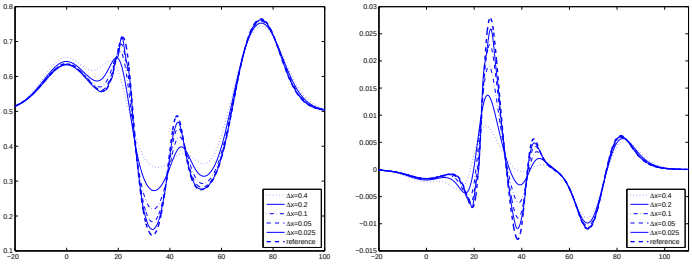

(c) $\mathcal{T}$ at $t=6$ (d) q at $t=6$

Figure 2: The density ρ, macroscopic momentum, the local temperature $\mathcal{T}$ and heat flux q of the 1D-1D Wigner equation with only the classical acceleration and without the scattering term on different spatial grids at $t=6$. The thick dashed line is the reference solution.

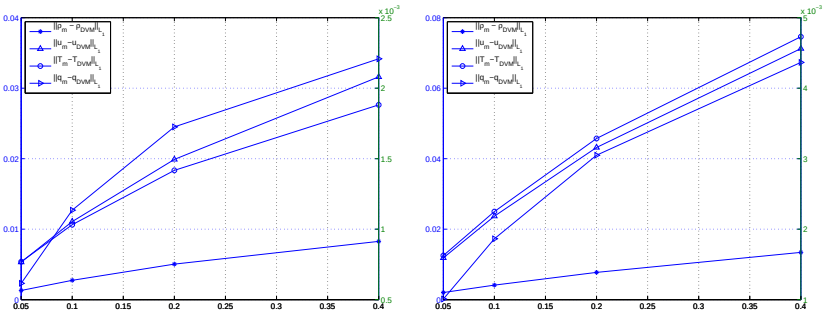

(a) $t=3$ (b) $t=6$

Figure 3: The L_1 error of the density ρ, macroscopic momentum u, local temperature $\mathcal{T}$ and heat flux q between the moment method using different spatial grid sizes and the discrete velocity method in the case of the 1D-1D Wigner equation with only the classical acceleration and without the scattering term at $t=3$ and $t=6$. The x-axis is the spatial grid size Δx and the y-axis is the L_1 error. The right y-axis is for heat flux.

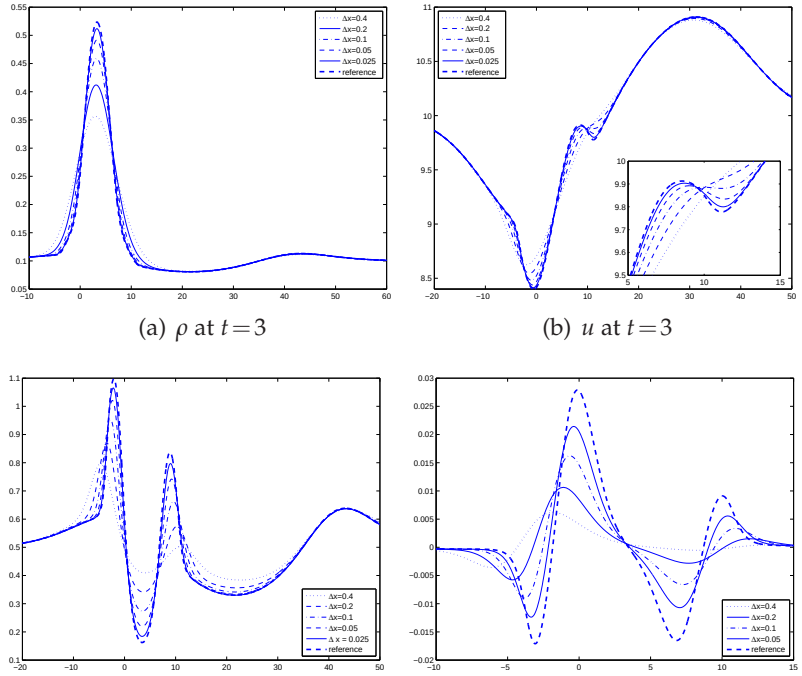

(a) ρ at $t=3$ (b) u at $t=3$

(c) $\mathcal{T}$ at $t=3$ (d) q at $t=3$

Figure 4: The density ρ, macroscopic momentum u, local temperature $\mathcal{T}$ and heat flux q of the 1D-1D Wigner equation with only the classical acceleration and with the relaxation time $\tau=1/2$ on different spatial grid sizes at $t=3$. The thick dashed line is the reference solution.

number of moments is a easier task than the one without a scattering term. So here we would numerically solve the 1D-1D Wigner equation without the scattering term. We use a fixed grid size and range the number of moments from 5 to 25. ρ, u, $\mathcal{T}$ and q obtained by solving the moment system with different moments are plotted in Fig. 7.

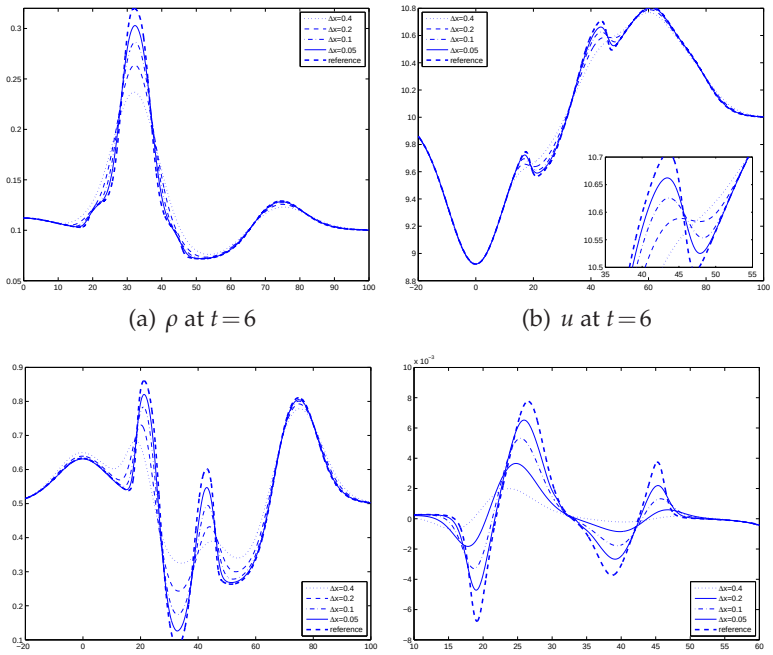

(a) ρ at $t=6$ (b) u at $t=6$

(c) $\mathcal{T}$ at $t=6$ (d) q at $t=6$

Figure 5: The density ρ, macroscopic momentum u, the local temperature $\mathcal{T}$ and heat flux q of the 1D-1D Wigner equation with only the classical acceleration and with the relaxation time $\tau=1/2$ on different spatial grid sizes at $t=6$. The thick dashed line is the reference solution.

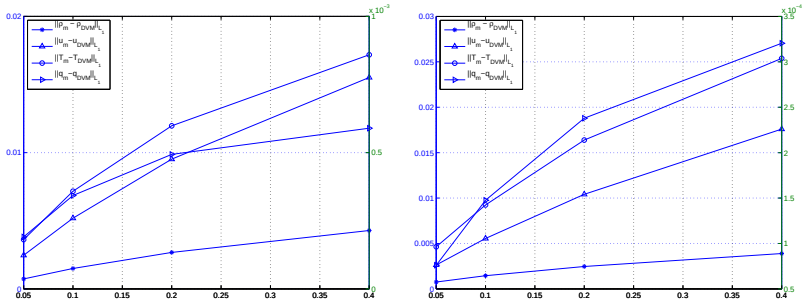

(a) $t=3$ (b) $t=6$

Figure 6: The L_1 error of the density ρ, macroscopic momentum u, local temperature $\mathcal{T}$ and heat flux q between the moment method using different spatial grid sizes and the discrete velocity method in the case of the 1D-1D Wigner equation with only the classical acceleration and with the relaxation time $\tau=1/2$ at $t=3$ and $t=6$. The x-axis is the spatial grid size Δx and the y-axis is the L_1 error.

Observing Fig. 7, we find out that if the number of moments is very small, significant oscillations of ρ, u, $\mathcal{T}$ and q appear in part of the domain. But with the increasing number of moments, the moment system can resolve the distribution function in the microscopic velocity space, the oscillations are gradually alleviated, and the results of the moment method converge to the solution obtained by the discrete velocity method.

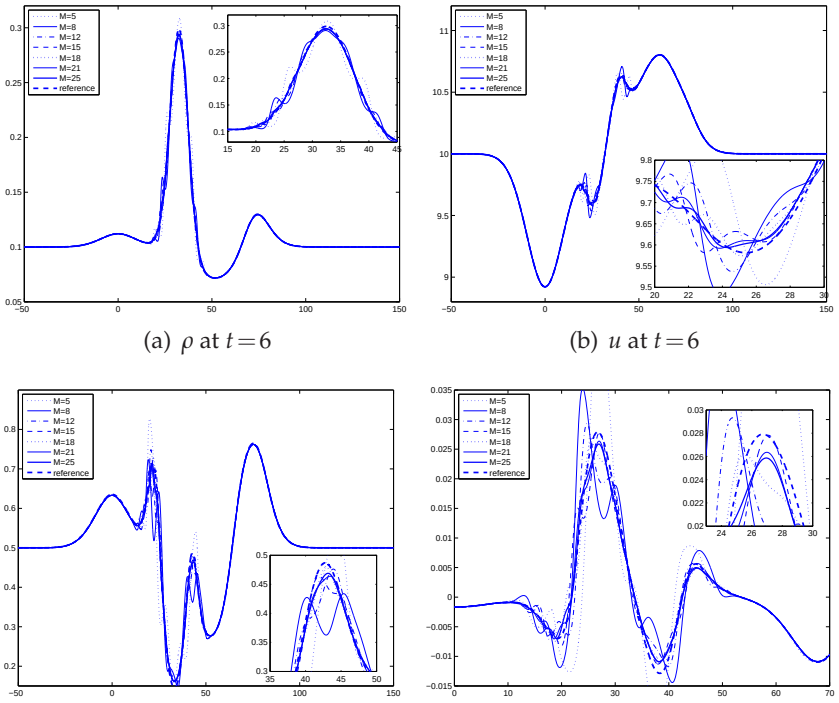

(a) ρ at $t=6$ (b) u at $t=6$

(c) $\mathcal{T}$ at $t=6$ (d) q at $t=6$

Figure 7: The density ρ, macroscopic momentum u, the local temperature $\mathcal{T}$ and heat flux q on different number of moments M of the 1D-1D Wigner equation with only the classical acceleration and without the scattering term at $t=6$. The thick dashed line is the reference solution.

4.2 Numerical convergence study for quantum system

As we have done to the Boltzmann equation in the previous section, we do the same study to the Wigner equation in this subsection. The numerical convergence of the moment method is studied when it is applied on the 1D-1D Wigner equation with the quantum acceleration term. We first examine the numerical convergence on different spatial grid size. The same number of moments and grid size of mesh as in the classical system are used here. The results of the density ρ, macroscopic momentum u, local temperature $\mathcal{T}$ and heat flux q at $t=3$ and $t=6$ without and with the scattering term are plotted in Figs. 8, 9, 11 and 12. Here, the same relaxation time $\tau=1/2$ is chosen. From Figs. 8, 9, 11 and 12, we can find that the total effect of the potential on the particles in the quantum system is smaller than that in the classical system. As to the convergence, it is obvious that the results of the moment method is converging to the result of the discrete velocity method with the decreasing of the spatial grid size. In Figs. 10 and 13, the L_1 error of ρ, u, $\mathcal{T}$ and q between the moment method and the discrete velocity method at $t=3$, and $t=6$ are plotted. The error is about linearly converging to zero with the decreasing of the spatial grid size.

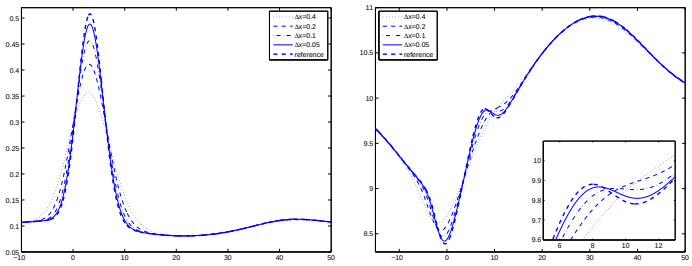

(a) ρ at $t=3$ (b) u at $t=3$

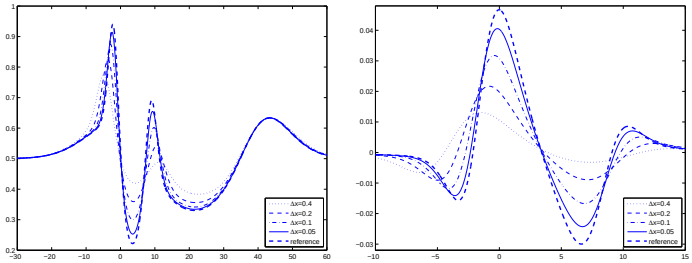

(c) $\mathcal{T}$ at $t=3$ (d) q at $t=3$

Figure 8: The density ρ, macroscopic momentum u, local temperature $\mathcal{T}$ and heat flux q of the 1D-1D Wigner equation with the quantum acceleration and without the scattering term on different spatial grids at $t=3$. The thick dashed line is the reference solution.

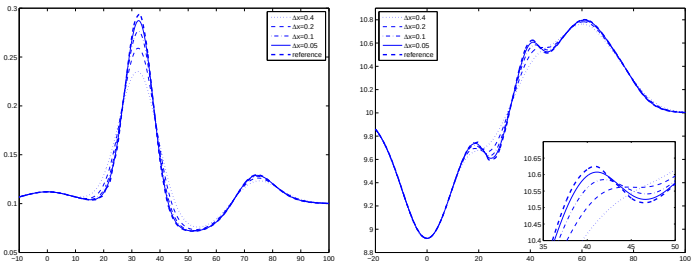

(a) ρ at $t=6$ (b) u at $t=6$

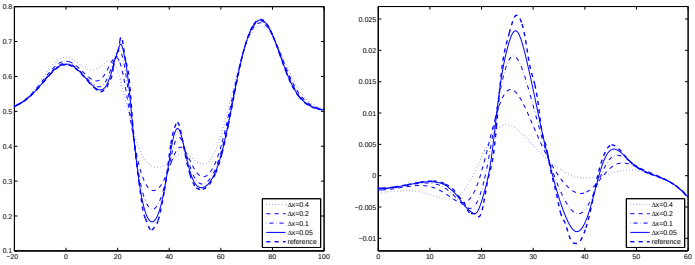

(c) $\mathcal{T}$ at $t=6$ (d) q at $t=6$

Figure 9: The density ρ, macroscopic momentum u, local temperature $\mathcal{T}$ and heat flux q of the 1D-1D Wigner equation with the quantum acceleration and without the scattering term on different spatial grids at $t=6$. The thick dashed line is the reference solution.

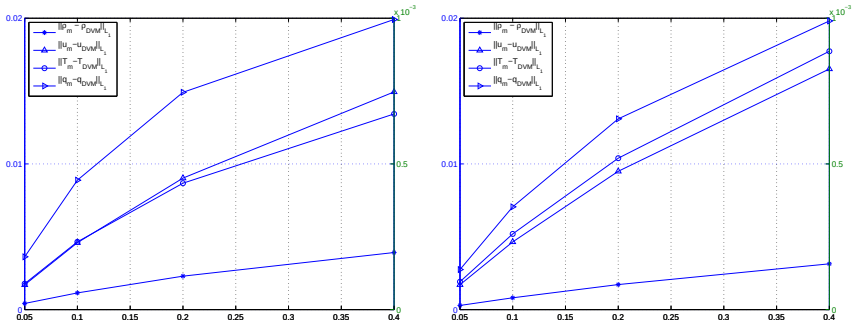

(a) $t=3$ (b) $t=6$

Figure 10: The L_1 error of the density ρ, macroscopic momentum u and the local temperature $\mathcal{T}$ between the moment method using different spatial grid sizes and the discrete velocity method in the case of the 1D-1D Wigner equation with the quantum acceleration and without the scattering term at $t=3$ and $t=6$. The x-axis is the spatial grid size Δx and the y-axis is the L_1 error.

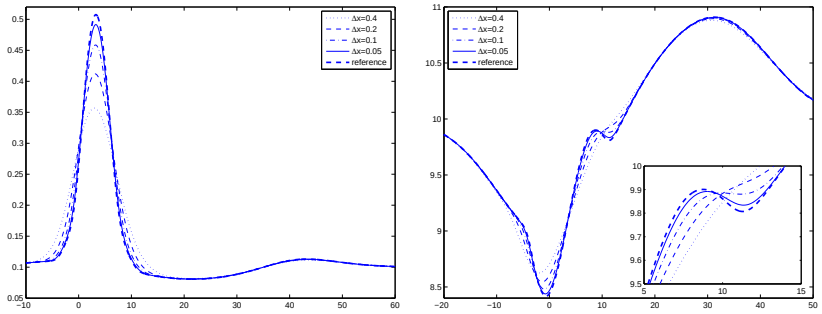

(a) ρ at $t=3$ (b) u at $t=3$

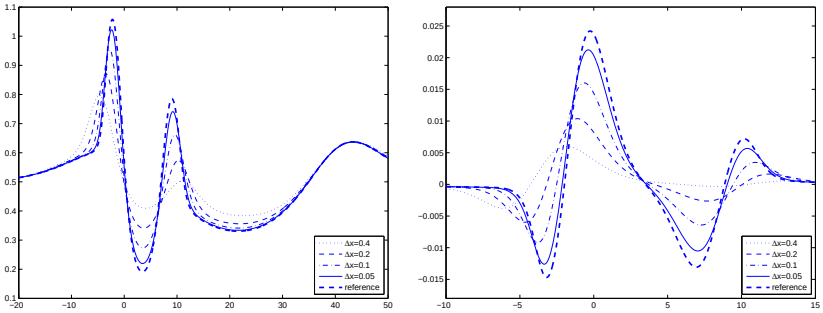

(c) $\mathcal{T}$ at $t=3$ (d) q at $t=3$

Figure 11: The density ρ, macroscopic momentum u, local temperature $\mathcal{T}$ and heat flux q of the 1D-1D Wigner equation with the quantum acceleration and with the relaxation time $\tau=1/2$ on different spatial grids at $t=3$. The thick dashed line is the reference solution.

The numerical convergence in terms of the number of moments is also studied then. Again the 1D-1D Wigner equation without the scattering term is numerically solved. In Fig. 14, the numerical results of ρ, u, $\mathcal{T}$ and q with the number of moments varying form

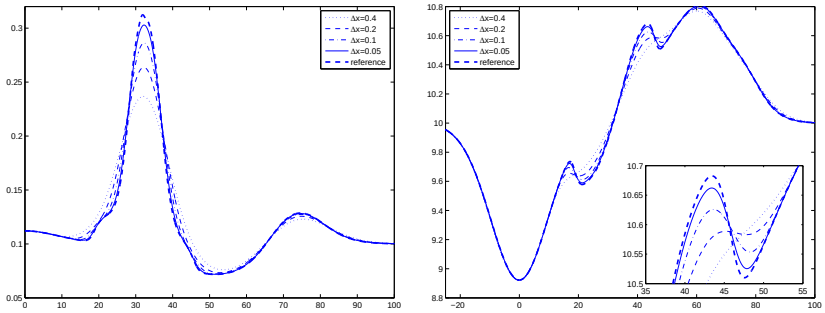

(a) ρ at $t=6$ (b) u at $t=6$

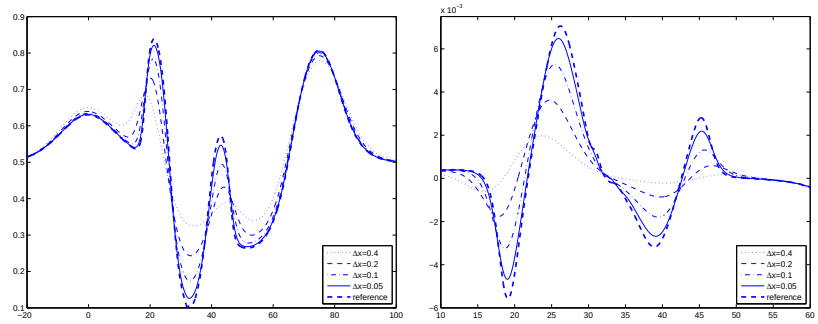

(c) $\mathcal{T}$ at $t=6$ (d) q at $t=6$

Figure 12: The density ρ, macroscopic momentum u, local temperature $\mathcal{T}$ and heat flux q of the 1D-1D Wigner equation with the quantum acceleration and with the relaxation time $\tau=1/2$ on different spatial grids at $t=6$. The thick dashed line is the reference solution.

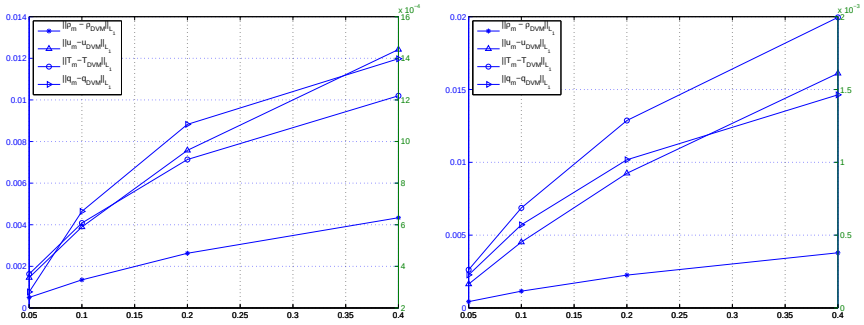

(a) $t=3$ (b) $t=6$

Figure 13: The L_1 error of the density ρ, macroscopic momentum u, local temperature $\mathcal{T}$ and heat flux q between the moment method using different number of the spatial grid size and the discrete method in the case of the 1D-1D Wigner equation with the quantum acceleration and with the relaxation time $\tau=1/2$ at $t=3$ and $t=6$. The x-axis is the spatial grid size Δx and the y-axis is the L_1 error. The right y-axis is for heat flux.

5 to 25, and with fixed spatial grid size are plotted. Similar to the result in the classical system, the oscillations are also appearing when the number of moments is small and are disappearing with the increasing of the number of moments. Additionally, the results

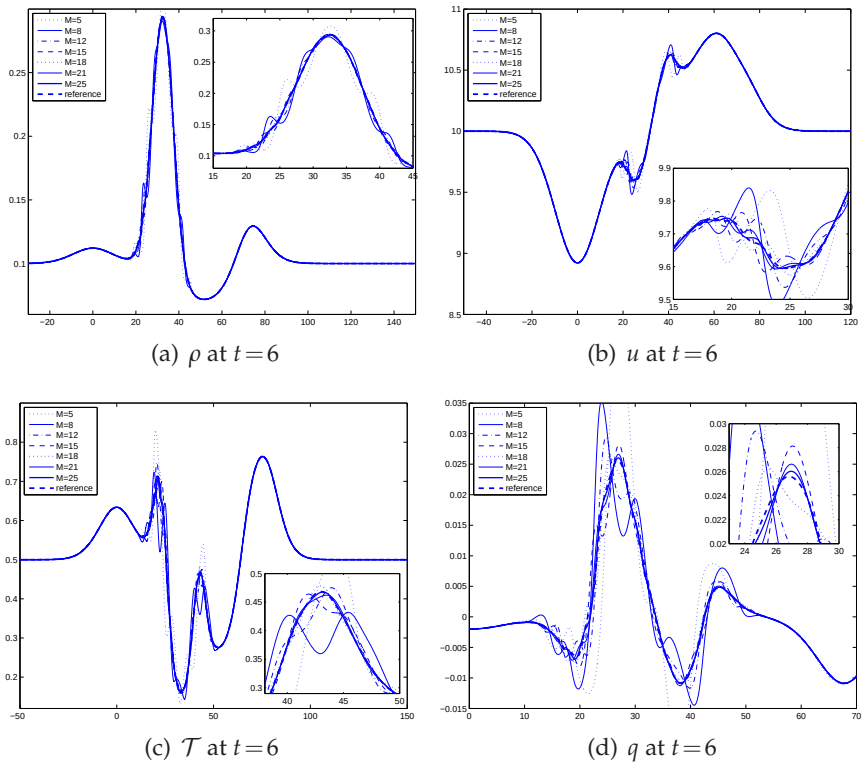

(a) ρ at $t=6$ (b) u at $t=6$

(c) $\mathcal{T}$ at $t=6$ (d) q at $t=6$

Figure 14: The density ρ, macroscopic momentum u, the local temperature $\mathcal{T}$ and heat flux q of the 1D-1D Wigner equation with the quantum acceleration term and without the scattering term on different number of moments at $t=6$. The thick dashed line is the reference solution.

of the moment method are also converging to the result of the discrete velocity method with the increasing of the number of moments as well.

4.3 Total energy variation

It has been proved in Theorem 3.1 that the mass and the momentum are conserved by our numerical scheme, while the total energy variation is of order $\mathcal{O}(\Delta t^2)$ in one time step. Thus, the variation of the total energy up to time scale $\mathcal{O}(1)$ is of order $\mathcal{O}(\Delta t)$. The 1D-1D Wigner equation with only the classical acceleration and without the scattering term is computed here to examine the behavior of the total energy variation. The mesh size $\Delta x = 0.4,\ 0.2,\ 0.05,\ 0.025$ are used here. With a fixed CFL number, the time step length Δt are then used accordingly. The variation of the total energy in time in these different setups are plotted in Fig. 15. It is clear that the variation of the total energy of the numerical solution produced by our method is almost linear in time. For a fixed t, the variation of the total energy is linear in terms of Δt. The variation of the total energy for the other computational configurations has the similar behavior. We omit these results to avoiding redundancy.

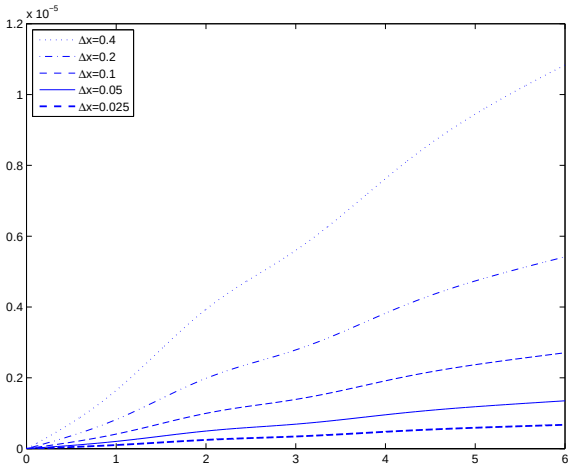

Figure 15: The variation of the total energy $\mathcal{E}_{total}$ of the 1D-1D Wigner equation with only the classical acceleration and without the scattering term. The x-axis is time and the y-axis is $(\mathcal{E}_{total}(t^k)-\mathcal{E}_{total}(0)-\sum_{j=1}^{k-1}\mathcal{W}_h(t^j))/\mathcal{E}_{total}(0)$.

5 Concluding remarks

The NRxx method for the Boltzmann equation in [8] is extended to solve the moment system of the Wigner equation. The numerical convergence of this method in terms of both the spatial grid size and the number of moments is verified in the classical system and the quantum system of the Wigner equation. It is validated by the numerical results that the moment system is an efficient model for the Wigner equation. With great efficiency improvement achieved by the moment method compared with the discrete velocity method, we are now on the way to carry out semiconductor device simulation modelled by the Wigner equation.

Acknowledgments

This research of R. Li was supported in part by the National Basic Research Program of China (2011CB309704) and Fok Ying Tong Education and NCET in China. T. Lu was supported in part by the NSFC (11011130029, 91230107) and by SRF for ROCS, SEM.

References

[1] A. Arnold and C. Ringhofer. An operator splitting method for the Wigner-Poisson problem. SIAM Journal on Numerical Analysis, 33(4):pp. 1622–1643, 1996.

[2] J.D. Au, H. Struchtrup, and M. Torrilhon. ET_{XX} — an equation generator for extended thermodynamics. Source available on request via `M.Torrilhon@vt.tu-berlin.de`.

[3] P. L. Bhatnagar, E. P. Gross, and M. Krook. A model for collision processes in gases. I. small amplitude processes in charged and neutral one-component systems. Phys. Rev., 94(3):511–525, 1954.
[4] Z. Cai, Y. Fan, and R. Li. Globally hyperbolic regularization of Grad's moment system. To appear in Comm. Pure Appl. Math., 2012.
[5] Z. Cai, Y. Fan, and R. Li. Globally hyperbolic regularization of Grad's moment system in one dimensional space. Comm. Math Sci., 11(2):547–571, 2013.
[6] Z. Cai, Y. Fan, R. Li, T. Lu, and Y. Wang. Quantum hydrodynamics models by moment closure of Wigner equation. J. Math. Phys., 53:103503, 2012.
[7] Z. Cai and R. Li. Numerical regularized moment method of arbitrary order for Boltzmann-BGK equation. SIAM J. Sci. Comput., 32(5):2875–2907, 2010.
[8] Z. Cai, R. Li, and Z. Qiao. Globally hyperbolic regularized moment method with applications to microflow simulation. Computer and Fluids, 81:95–109, 2013.
[9] Z. Cai, R. Li, and Y. Wang. An efficient NRxx method for Boltzmann-BGK equation. J. Sci. Comput., 50(1):103–119, 2012.
[10] Z. Cai, R. Li, and Y. Wang. Numerical regularized moment method for high Mach number flow. Commun. Comput. Phys., 11(5):1415–1438, 2012.
[11] Z. Cai, R. Li, and Y. Wang. Solving Vlasov equation using NRxx method. To appear in SIAM J. Sci. Comput., 2012.
[12] P. Degond, F. Méhats, and C. Ringofer. Quantum energy-transport and drift-diffusion models. J. Stat. Phys., 118:625–667, 2005.
[13] P. Degond and C. Ringhofer. Quantum moment hydrodynamics and the entropy principle. J. Stat. Phys., 112:587–628, 2003.
[14] D.K. Ferry and S. M. Goodnick. Transport in Nanostructures. Cambridge Univ. Press, Cambridge, U.K, 1997.
[15] W.R. Frensley. Wigner function model of a resonant-tunneling semiconductor device. Phys. Rev. B, 36:1570–1580, 1987.
[16] C.L. Gardner. The quantum hydrodynamic model for semiconductor devices. SIAM J. Appl. Math., 54:409–427, 1994.
[17] T. Goudon and S. Lohrengel. On a discrete model for quantum transport in semi-conductor devices. Transp. Theory Stat. Phys., 31(4-6):471–490, 2002.
[18] T. Goudon. Analysis of a semidiscrete version of the Wigner equation. SIAM J. Numerical Analysis, 40(6):2007–2025, 2002.
[19] H. Grad. On the kinetic theory of rarefied gases. Comm. Pure Appl. Math., 2(4):331–407, 1949.
[20] H. Grad. The profile of a steady plane shock wave. Comm. Pure Appl. Math., 5(3):257–300, 1952.
[21] M. Hillery, R.F. ÓConnell, M.O. Scully, and E.P. Wigner. Distribution functions in physics: Fundamentals. Physics Reports, 106(3):121–167, 1984.
[22] X. Hu, S. Tang, and M. Leroux. Stationary and transient simulations for a one-dimensional resonant tunneling diode. Commun. Comput. Phys., 4(5):1034–1050, 2008.
[23] K. L. Jensen and F.A. Buot. Numerical simulation of intrinsic bistability and high-frequency current oscillations in resonant tunneling structures. Phys. Rev. Lett., 66:1078–1081, Feb 1991.
[24] K.L. Jensen and F.A. Buot. Numerical aspects on the simulation of IV characteristics and switching times of resonant tunneling diodes. J. Appl. Phys., 67:2153–255, 1990.
[25] S. Jin and M. Slemrod. Regularization of the Burnett equations via relaxation. J. Stat. Phys,

103(5–6):1009–1033, 2001.
[26] A. Jüngel. A note on current-voltage characteristics from the quantum hydrodynamic equations for semiconductors. Appl. Math. Lett., 10(4):29–34, 1997.
[27] Ansgar Jngel and Shaoqiang Tang. Numerical approximation of the viscous quantum hydrodynamic model for semiconductors. Appl. Numer. Math., 56(7):899 – 915, 2006.
[28] K.-Y. Kim and Byoungho Lee. On the high order numerical calculation schemes for the wigner transport equation. Solid-State Electronics, 43(12):2243 – 2245, 1999.
[29] C. D. Levermore. Moment closure hierarchies for kinetic theories. J. Stat. Phys., 83(5–6):1021–1065, 1996.
[30] T. Lu, G. Du, X. Liu, and P. Zhang. A finite volume method for the multi subband Boltzmann equation with realistic 2D scattering in DG MOSFETs. Commun. Comput. Phys., 10:305–338, 2011.
[31] G. Dal Maso, P. G. LeFloch, and F. Murat. Definition and weak stability of nonconservative products. J. Math. Pures Appl., 74(6):483–548, 1995.
[32] M. Nedialkov, H. Kosina, S. Selberherr, C. Ringhofer, and D. K. Ferry. Unified particle approach to wigner-boltzmann transport in small semiconductor devices. Physical Review B, page 115319, 2004.
[33] S. Rhebergen, O. Bokhove, and J. J. W. van der Vegt. Discontinuous Galerkin finite element methods for hyperbolic nonconservative partial differential equations. J. Comput. Phys., 227(3):1887–1922, 2008.
[34] C. Ringhofer. A spectral method for the numerical solution of quantum tunneling phenomena. SIAM J. Num. Anal., 27:32–50, 1990.
[35] S. Shao, T. Lu, and W. Cai. Adaptive conservative cell average spectral element methods for transient Wigner equation in quantum transport. Commun. Comput. Phys., 9:711–739, 2011.
[36] G. Strang. On the construction and comparison of difference schemes. SIAM J. Numer. Anal., 5(3):506–517, 1968.
[37] H. Struchtrup. Stable transport equations for rarefied gases at high orders in the Knudsen number. Phys. Fluids, 16(11):3921–3934, 2004.
[38] H. Struchtrup and M. Torrilhon. Regularization of Grad's 13 moment equations: Derivation and linear analysis. Phys. Fluids, 15(9):2668–2680, 2003.
[39] M. Torrilhon. Regularized 13-moment-equations. In M. S. Ivanov and A. K. Rebrov, editors, Rarefied Gas Dynamics: 25th International Symposium, 2006.
[40] M. Torrilhon, J. D. Au, and H. Struchtrup. Explicit fluxes and productions for large systems of the moment method based on extended thermodynamics. Cont. Mech. and Ther., 15(1):97–111, 2002.
[41] E. Wigner. On the quantum correction for thermodynamic equilibrium. Phys. Rev., 40(5):749–759, Jun 1932.
[42] P.J. Zhao, D.L. Woolard, and H.L. Cui. Multisubband theory for the origination of intrinsic oscillations within double-barrier quantum well systems. Phys. Rev. B, 67:085312, Feb 2003.
[43] J.-R. Zhou and D.K. Ferry. Simulation of ultra-small GaAs MESFET using quantum moment equations. IEEE Trans. Electron Devices, 39(3):473–478, 1992.